

# Atomistic modeling of functionalized magnetite surfaces with oxidation states

Emre Gürsoy

*Institute of Interface Physics, Hamburg University of Technology, Hamburg, Germany*

Gregor B. Vonbun-Feldbauer\*

*Institute of Advanced Ceramics, Hamburg University of Technology, Hamburg, Germany and*

*Institute of Interface Physics, Hamburg University of Technology, Hamburg, Germany*

Robert H. Meißner

*Institute of Interface Physics, Hamburg University of Technology, Hamburg, Germany and*

*Institute of Surface Science, Helmholtz-Zentrum Hereon, Geesthacht, Germany*

(Dated: March 6, 2025)

## Abstract

Understanding the atomic structure of magnetite-carboxylic acid interfaces is crucial for tailoring nanocomposites involving this interface. We present a Monte Carlo (MC)-based method utilizing iron oxidation state exchange to model magnetite interfaces with tens of thousands of atoms—scales typically inaccessible by electronic structure calculations. By comparing the binding site preferences of carboxylic acids obtained from electronic structure calculations, we validated the accuracy of our method. We found that the oxidation state distribution, and consequently binding site preference, depend on coverage and surface thickness, with a critical thickness signaling the transition from layered to bulk-like oxidation states. The method presented here needs no interface specific parameterization, ensuring seamless compatibility with popular bimolecular force fields providing transferability, and simplifying the study of magnetite interfaces in general.

Magnetite is a biocompatible material that finds various applications spanning from drug delivery<sup>1</sup>, therapeutic agents<sup>2</sup> to magnetic resonance imaging (MRI)<sup>3</sup>. Magnetite interfaces play a crucial role in building a cleaner and more sustainable future, including pesticides removal from water<sup>4</sup>, Fischer–Tropsch synthesis<sup>5</sup>, and the water-gas shift reaction<sup>6</sup>. Moreover, functionalized magnetite nanoparticles, e.g. with oleic acid, serve as fundamental building blocks for hierarchical nanocomposites<sup>7,8</sup>. Those nanocomposites have exceptional mechanical properties<sup>9</sup> that can be fine-tuned by modifying nanoparticle morphology<sup>10,11</sup>, introducing additional hierarchical levels<sup>12</sup> or altering ligand reactivity<sup>13</sup>.

In general, magnetite exhibits two dominant surface facets, the (001) and (111) surfaces, which are often observed at magnetite nanoparticles due to their low surface energies.<sup>10</sup> The stability and morphology of the (111) surface strongly depends on the surrounding environment and the specific preparation conditions.<sup>14–19</sup> For the (001) surface two surface models are commonly used, the distorted bulk truncation (DBT)<sup>20</sup> and the subsurface cation vacancy (SCV) reconstruction<sup>21</sup>. While the SCV reconstruction is usually found under ultrahigh vacuum conditions, the DBT can be stabilized in the presence of adsorbates like hydrogen and formic acid.<sup>22–25</sup> On (001) magnetite surfaces under UHV conditions, formic acid (HCOOH) undergoes dissociative adsorption and dissociates into a formate (HCOO<sup>-</sup>) and a proton (H<sup>+</sup>), where the formate prefers a bidentate binding mode. On the (001)-DBT surface, two distinct adsorption sites are observed: formate either adsorbs next to an Fe<sub>tet</sub> ion, the “tet” adsorption site, or in a region between two Fe<sub>tet</sub> ions, the “int” adsorption site (cf. Fig. 1).<sup>23,24,26</sup> To harness the potential of magnetite based nanocomposites, intensive efforts were made to shed light on magnetite interfaces<sup>27</sup>, particularly those involving formic acids serving as the archetype for carboxylic ligands<sup>18,23,24,26</sup>. Although this work focuses on the (001)-DBT surface as a model system due to the availability of high-quality experimental and computational data, the method described herein is considered to be applicable to any magnetite-organic interface.

In atomistic models of magnetite interfaces, atoms are often described by point charges, whereby the parameters describing these point charges are tailored either to specific interfaces, such as carboxylic acids<sup>26</sup> and phosphonic acids<sup>4</sup>, or to specific morphologies, such as nanoparticles<sup>28,29</sup>. The parametrization of force fields is typically done on the basis of electronic structure calculations or experiments.

The dissociation of carboxylic acids upon adsorption onto magnetite requires a specific pa-

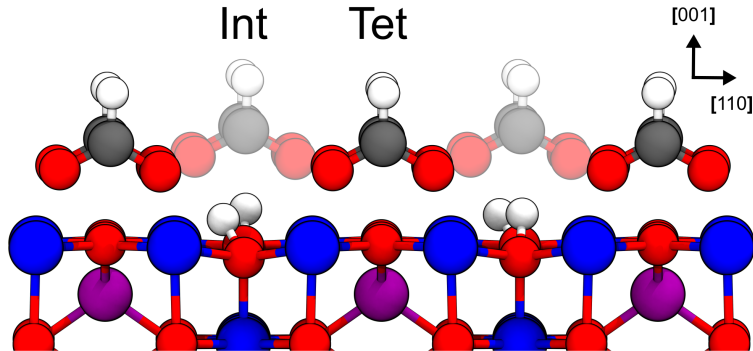


FIG. 1. **Formic acid adsorption sites on (001) magnetite surface.** Adsorption sites, “tet” and “int”, are highlighted. Color code:  $\text{Fe}_{\text{oct}}^{3+}$  – dark blue,  $\text{Fe}_{\text{tet}}^{3+}$  – purple, O – red, H – white, C – gray.

parameterization of the proton transfer. Common drawbacks of many force fields are incorrect energies and the frequent appearance of excess charges in the case of chemical reactions.<sup>30,31</sup> The latter are often compensated for by adding or removing charge carriers within the system to maintain charge neutrality. This can be achieved, e.g., by adding ions,<sup>32</sup> dissociating water on the surface to form hydroxyl groups<sup>33</sup>, distribution of the excess charge on some atoms<sup>26</sup> or the creation of deprotonated charged surface sites.<sup>30</sup> While adding or removing charge carriers secures the charge neutrality, it changes the overall composition of the system.

Using standard GAFF<sup>34,35</sup> and ClayFF<sup>36</sup> partial charges for formic acid and formate, and magnetite, respectively (cf. Konuk et al.<sup>26</sup>) results in a negatively charged system: Formate contributes  $-1.0e$  to the overall charge, hydroxyl hydrogen  $\text{H}_\text{O}$  contributes  $+0.425e$  and the bridging oxygen (O) in magnetite turns into a hydroxyl oxygen ( $\text{O}_\text{H}$ ) changing its charge by  $+0.05e$ , where  $e$  represents the elementary charge. This results in an excess charge of  $-0.525e$  (cf.  $\Delta q$  in Fig. 2b). Previously the necessary compensation charge was distributed among the atoms in proximity of the reaction site based on reference density functional theory (DFT) calculations.<sup>26,27</sup> This makes the parametrization interface specific and limits its transferability.

We present a simple but effective atomistic simulation method that neither requires additional charge carriers nor interface specific magnetite parameters which, e.g., depend on the specific surface<sup>26</sup>. This method is based on three steps: (1) including the charge transfer from adsorbates to magnetite by oxidizing  $\text{Fe}^{2+}$  ions (cf. Fig. 2a, b), (2) minimizing

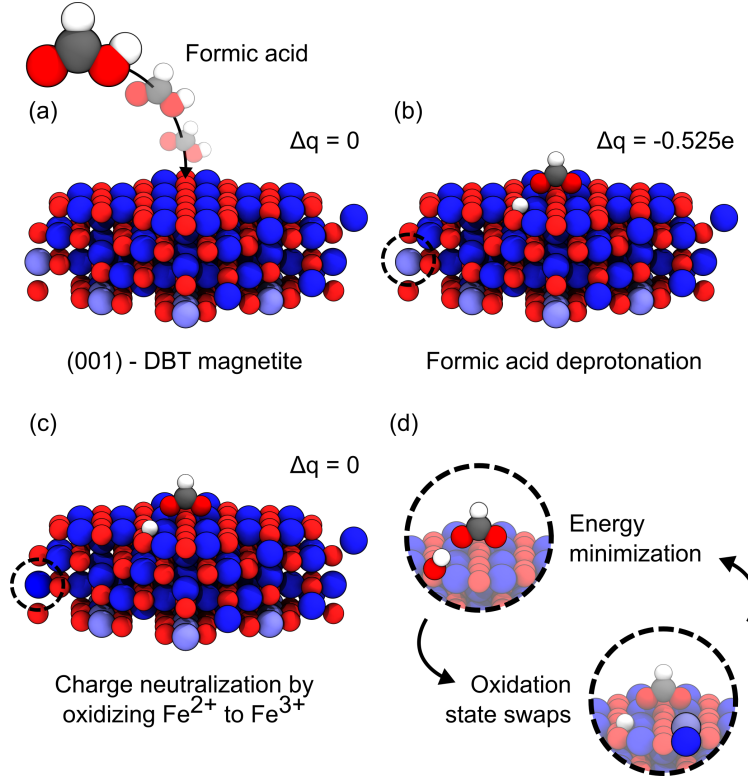


FIG. 2. **Formic acid adsorption and oxidation state minimization at magnetite interface.**

(a) Schematic representation of formic acid adsorption on magnetite surface. The overall system is charge neutral. (b) Formic acid deprotonates to formate and a hydrogen. And as the result, the total charge of the system (adsorbate + magnetite) becomes slightly negative ( $-0.525e$ ). (c) By oxidizing an Fe<sup>2+</sup> to Fe<sup>3+</sup> the system becomes charge neutral again. (d) Through a cyclic process of oxidation state swaps and energy minimization, the minimized oxidation state configurations are obtained. Color code: Fe<sup>3+</sup><sub>oct</sub> – dark blue, Fe<sup>2+</sup><sub>oct</sub> – light blue, O – red, H – white and C – gray.

the potential energy of the adsorbates, (3) using Monte Carlo (MC) to swap the oxidation states of the Fe ions. Steps (2) and (3) are carried out repeatedly until convergence (cf. Fig. 2d). This process is referred to as “oxidation state minimization”, as it entails forcing the oxidation states of Fe ions to adapt to the adsorbate geometry. Details of oxidation state minimization are given in the Supporting Information (SI). This represents an extension of our previous method<sup>37</sup> which was developed for investigating bulk magnetite, and unfunctionalized magnetite surfaces and nanoparticles.

More specifically, the excess charge in step (1) from the dissociation of a formic acid on its respective adsorption site is compensated by oxidizing an Fe<sup>2+</sup> → Fe<sup>3+</sup>, where  $q^{3+} - q^{2+} =$

0.525  $e$ . This oxidation state change ensures charge neutrality (cf.  $\Delta q$  in Fig. 2c) of the overall system when formic acid dissociates and a hydroxyl is formed on the surface. Note that in general, we assume that the missing  $\text{Fe}^{2+}$  on the octahedral places due to surfaces and adsorption are compensated and, e.g., found in defects in the bulk of real systems. This assumption may not hold for small systems where the  $\text{Fe}^{2+}/\text{Fe}^{3+}$  ratio is too far from ideal stoichiometry. Force field parameters describing magnetite, formate and surface hydroxides are presented in Tab. SI1. For comparison DFT calculations were performed on functionalized magnetite slabs. Compared to our previous formic acid adsorption studies<sup>24,26</sup>, we increased the system size and removed symmetry constraints following our work on bare magnetite surface.<sup>37</sup> Details on the DFT calculations can be found in the Supporting Information (SI).

Oxidation state minimization was applied on functionalized magnetite slabs with thickness ranging from 9L ( $\approx 1$  nm) to 65L ( $\approx 7$  nm), where L stands for iron layers. Formate molecules are located at “tet” and “int” binding sites for both half and full formate coverage. Full coverage is defined here as every surface Fe atom having a bond to a formate O atom. Some structures are shown as examples in Fig. 3. It is important to note that both top and bottom magnetite surfaces of the slab used in the simulations are functionalized. Due to the long-range electrostatics, functionalizing only one surface results in an unwanted dipole and in an unrealistic asymmetric oxidation state distribution (cf. Fig. SI1). At room temperature, all  $\text{Fe}_{\text{tet}}$  in magnetite are usually  $\text{Fe}^{3+}$ . Hence, all  $\text{Fe}_{\text{tet}}$  are fixed to  $\text{Fe}^{3+}$  and excluded from the oxidation swaps. Consequently, we focus only on  $\text{Fe}_{\text{oct}}$  which can be both  $\text{Fe}^{3+}$  or  $\text{Fe}^{2+}$ . At elevated temperatures this is not be a reasonable approach and swaps should also be done for  $\text{Fe}_{\text{tet}}$ .<sup>38</sup> To assess whether a given layer exhibits a bulk-like oxidation state distribution with  $n_{\text{Fe}_{\text{oct}}^{3+}}/n_{\text{Fe}_{\text{oct}}} = 0.5$  or not, the  $\text{Fe}^{3+}$  ratio within each  $\text{Fe}_{\text{oct}}$  layer was calculated and is shown in Fig. 3. Since in the DFT calculations the OH molecules at the top and bottom interfaces face in opposite directions, following the point symmetry of the magnetite slab, we focus on these for consistency. Nevertheless, we have checked in Figs. SI2 and SI3 if the direction of the surface hydroxyls has an effect on our simulations. No significant differences were found. Atomistic structures of both same-directional and opposite-directional OH models can be seen in Fig. SI4.

At 17L and half formate coverage, the first two  $\text{Fe}_{\text{oct}}$  layers at the interface only contain  $\text{Fe}^{3+}$  oxidation state (cf. Fig. 3a). These  $\text{Fe}_{\text{oct}}$  layers at the interface which are dominated

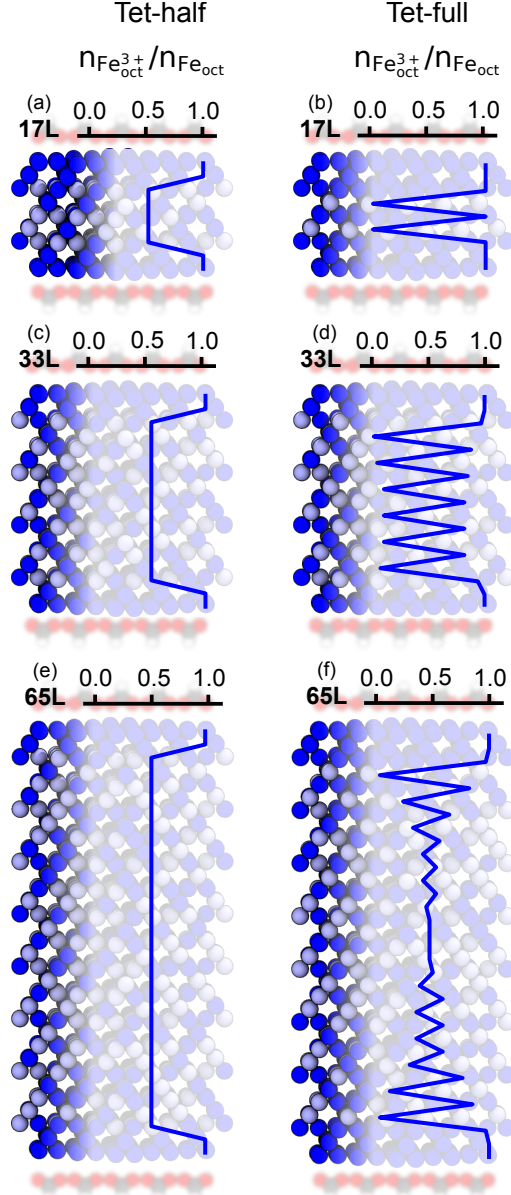


FIG. 3. **Oxidation state distribution of oxidation state minimized formate-magnetite interfaces.** Formate binding site (tet) and coverage ratio (half and full) are given in the title.  $n_{\text{Fe}_{\text{oct}}^{3+}}/n_{\text{Fe}_{\text{oct}}}$  ratio within each octahedral layer is denoted by  $n_{\text{Fe}_{\text{oct}}^{3+}}/n_{\text{Fe}_{\text{oct}}}$ . Number of atomic layers is indicated in the top-left corner.  $\text{Fe}_{\text{tet}}$ , O (magnetite),  $\text{O}_{\text{H}}$  and  $\text{H}_{\text{O}}$  are omitted. Color code:  $\text{Fe}_{\text{oct}}^{3+}$  – dark blue,  $\text{Fe}_{\text{oct}}^{2+}$  – light blue,  $\text{O}_{\text{C}}$  – red,  $\text{H}_{\text{C}}$  – white and  $\text{C}_{\text{C}}$  – gray.

by the  $\text{Fe}^{3+}$  are referred to as “surface layers”. The dominance of  $\text{Fe}^{3+}$  at surface layers is frequently observed, as in bare magnetite<sup>33,37,39</sup> and at magnetite / carboxylic acid interfaces<sup>24,26</sup>. At full coverage, the number of surface layers increases to three (cf. Fig. 3b).

This pattern continues up to magnetite slabs with 33L: two and three surface layers at half and full coverage, respectively. At full coverage, as there are more negatively charged adsorbates and more  $\text{Fe}^{3+}$  ions due to our charge neutrality approach (cf. Fig. 2c), a greater amount of  $\text{Fe}^{3+}$  are attracted to the interface, thus increasing the surface layer thickness. The surface layers no longer contain only  $\text{Fe}^{3+}$  for thicker slabs starting from 33L for full formate coverage. Some  $\text{Fe}^{2+}$  appear in the third surface layer (cf. Fig. 3d).

At half coverage bulk-like layers with  $n_{\text{Fe}_{\text{oct}}^{3+}}/n_{\text{Fe}_{\text{oct}}} = 0.5$  were observed for all slab thicknesses. In contrast, at full coverage we observe varying degrees of oxidation state layering. The layering becomes less pronounced with increasing slab thickness. For thin slabs, e.g. 17L in Fig. 3b, alternating layers exhibiting purely  $\text{Fe}^{3+}$  or  $\text{Fe}^{2+}$  were obtained in the simulations. This ideal layering disappears at 33L shown in Fig. 3d and a bulk-like region starts to emerge in the center of the slab at 65L given in Fig. 3f.

In order to check, if systems with non-ideal layering or a bulk-like region are energetically more favorable than ideal-layered, we forced thicker slabs to be in a layered configuration and compared resulting energies to those of oxidation state minimized structures in Fig 4a. Minimized structures become increasingly favorable with increasing thickness independent of the binding site.

Subsequently, we investigated the binding site preference, denoted as  $\Delta E_{\text{tet-int}}$ , of minimized structures and compared our findings with DFT calculations. At half coverage, we observed a strong “int” preference in Fig. 4b which is in good agreement with DFT calculations at 9L, 17L and 25L (cf. Tab SI2). During the oxidation state minimization at half coverage, formate molecules diffused from “tet” to “int” binding sites both at 25L and 33L thickness. We refrain from artificially fixing those and decided to exclude those results.

At full coverage an “int” preference was observed for the thinnest slab with 9L in Fig. 4c while DFT suggested “tet”. This could be attributed to the fact that our charge neutrality approach at 9L does not leave any  $\text{Fe}^{2+}$  ions after adsorption. Thicker slabs suggested a slight “tet” preference with 0.003 eV/formate, which agrees reasonably well with our previous empirical force field,<sup>26</sup> that also showed a “tet” preference by 0.02 eV/formate, and with our previous<sup>24</sup> and current DFT calculations, that also showed a “tet” preference by 0.041 eV/formate and 0.047 eV/formate, respectively. The “int” binding seems again to be more favorable for larger slabs at full coverage where 41L shows an unexpectedly strong preference of “int” binding. Problems with the minimization of such large system could

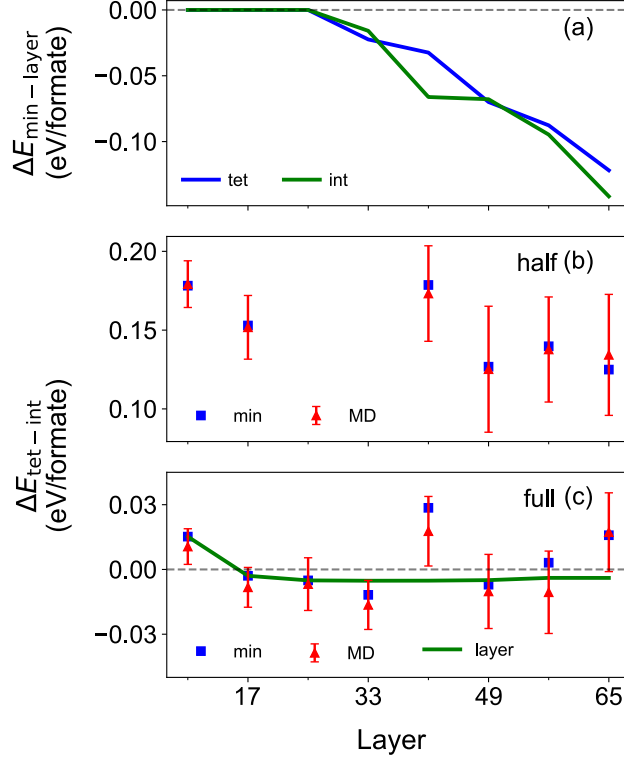


FIG. 4. (a) Energy difference between oxidation state minimized (min) and layered (layer) structures at full coverage with respect to surface thickness, at “tet” and “int” binding sites. (b) Binding site preference at half coverage for minimized and Molecular Dynamics (MD) resulted structures with respect to surface thickness. Error bars represent the standard deviations of MD. (c) Binding site preference at full coverage of minimized, layered, and Molecular Dynamics (MD) resulted structures with respect to surface thickness.

be a reason for this unexpected behavior. In enforced ideal-layered slabs, “tet” preference was observed regardless of the surface thickness (see the green line in Fig. 4c). The thickness of the slab, and hence the oxidation state distribution, seems to affect to some extent the adsorption behavior of formate, which is an effect previously not considered in many magnetite-adsorbate studies.

Next, we investigated the effects of finite temperatures on binding site preferences. Starting from the minimized structures, we applied Molecular Dynamics (MD) on the structures at 300 K, using the same settings as in our previous study<sup>37</sup>. For each structure we performed an MD simulation for 10 ns and used the last 5 ns to calculate the binding site preference shown in Fig. 4(b,c). The results indicate that room temperature has no significant influence



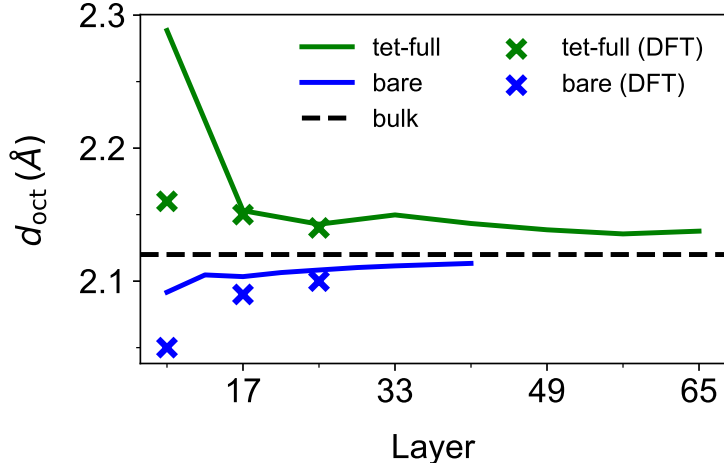


FIG. 5. **The average distance between octahedral layers ( $d_{\text{oct}}$ ) as a function of surface thickness.**  $d_{\text{oct}}$  values of oxidation state minimized structures: at full coverage with “tet” binding site, bare surface, and bulk magnetite, with DFT values given for comparison. Additional binding sites and coverages are shown in the Fig. SI5

on the binding site preferences. It should be noted that the oxidation state distribution was fixed in these MD simulations, since the effects of temperature on the adsorbates, such as changes in adsorption sites, were the main point of interest here.

For oxidation state minimized bare (001) DBT surfaces, the average distance between octahedral layers ( $d_{\text{oct}} = L_S / (n_{\text{oct}} - 1)$ ) increases with the slab thickness  $L_S$ , approaching the bulk value.<sup>37</sup>  $n_{\text{oct}}$  is the number of octahedral Fe layers. For functionalized surfaces, the opposite trend is observed. The average distance  $d_{\text{oct}}$  is above the bulk value and it decreases with slab thickness towards the bulk value (cf. Fig. 5). While at a bare surface, relaxations due to surface stresses are causing decreased interlayer distances, formic acid adsorption reduces these stresses and even yields an expansion of the slab. The largest deviation from the bulk value is observed between the first two octahedral Fe layers. This behavior is in very good agreement with our DFT calculations. For the 9L slab, deviations are observed due to limitations of the model as discussed above. Moreover, it has to be noted that the bare DBT surface is an artificial systems, since an SCV reconstruction would occur at such surfaces under typical experimental conditions. For the functionalized DBT surface, the results on the interlayer distances agree well with previous experimental observations.<sup>24</sup> The behaviors for all investigated coverages and adsorption sites are presented in the SI, see Fig. SI5.

In summary, we have shown that our oxidation state minimization method is capable of modeling magnetite-carboxylic acid interfaces and the results are in good agreement with electronic structure calculations and previous magnetite / carboxylic acid studies<sup>24,26</sup>. Particularly, no interface specific parametrization as used in our previous approach<sup>26</sup> is required, increasing the applicability and transferability of this approach. As a result, we have determined the number of layers required for a surface to have bulk-like layers in the middle of the slab. While at half coverage, bulk-like layers are observed even for thin slabs, at full coverage, much thicker slabs are needed. We have shown that the oxidation state distribution depends on the surface thickness and that the binding site preference is affected by the adsorbate coverage. The interlayer spacings for bare and adsorbate-covered surfaces are in very good agreement with DFT results.

The method presented here allows modeling much larger systems, and thus is suitable, e.g., for studying the mechanical and structural properties of functionalized magnetite based nanocomposites, which will be shown for example in an upcoming work.<sup>40</sup> In conclusion, the oxidation state minimization method, which is computationally much cheaper than electronic structure calculation, is a promising tool for modeling magnetite-carboxylic acid interfaces and magnetite-organic adsorbate interfaces in general.

## ACKNOWLEDGMENTS

This research was funded by the Deutsche Forschungsgemeinschaft (DFG, German Research Foundation) – SFB 986 – 192346071.

## SUPPORTING INFORMATION

Detailed information of the computational settings, electron localisation function using density functional theory, magnetite and carboxylic acid force field parameters.

---

\* gregor.feldbauer@tuhh.de

(1) Patitsa, M.; Karathanou, K.; Kanaki, Z.; Tzioga, L.; Pippa, N.; Demetzos, C.; Verganelakis, D. A.; Cournia, Z.; Klinakis, A. Magnetic nanoparticles coated with polyarabic

- acid demonstrate enhanced drug delivery and imaging properties for cancer theranostic applications. *Sci. Rep.* **2017**, *7*.
- (2) Wang, K.; Li, L.; Xu, X.; Lu, L.; Wang, J.; Wang, S.; Wang, Y.; Jin, Z.; Zhang, J. Z.; Jiang, Y. Fe<sub>3</sub>O<sub>4</sub>@Astragalus Polysaccharide Core-Shell Nanoparticles for Iron Deficiency Anemia Therapy and Magnetic Resonance Imaging in Vivo. *ACS Applied Materials & Interfaces* **2019**, *11*, 10452–10461.
  - (3) Stephen, Z. R.; Kievit, F. M.; Zhang, M. Magnetite nanoparticles for medical MR imaging. *Mater. Today* **2011**, *14*, 330–338.
  - (4) Park, H.; May, A.; Portilla, L.; Dietrich, H.; Münch, F.; Rejek, T.; Sarcletti, M.; Banspach, L.; Zahn, D.; Halik, M. Magnetite nanoparticles as efficient materials for removal of glyphosate from water. *Nature Sustainability* **2019**, *3*, 129–135.
  - (5) Cho, J. M.; Jeong, M. H.; Bae, J. W. Fischer–Tropsch synthesis on potassium-modified Fe<sub>3</sub>O<sub>4</sub> nanoparticles. *Research on Chemical Intermediates* **2015**, *42*, 335–350.
  - (6) Zhu, M.; Wachs, I. E. Iron-Based Catalysts for the High-Temperature Water–Gas Shift (HT-WGS) Reaction: A Review. *ACS Catalysis* **2015**, *6*, 722–732.
  - (7) Dreyer, A.; Feld, A.; Kornowski, A.; Yilmaz, E. D.; Noei, H.; Meyer, A.; Krekeler, T.; Jiao, C.; Stierle, A.; Abetz, V.; Weller, H.; Schneider, G. A. Organically linked iron oxide nanoparticle supercrystals with exceptional isotropic mechanical properties. *Nat. Mater.* **2016**, *15*, 522–528.
  - (8) Giuntini, D.; Torresani, E.; Chan, K. T.; Blankenburg, M.; Saviot, L.; Bor, B.; Domènech, B.; Shachar, M.; Müller, M.; Olevsky, E. A.; Garay, J. E.; Schneider, G. A. Iron oxide-based nanostructured ceramics with tailored magnetic and mechanical properties: development of mechanically robust, bulk superparamagnetic materials. *Nanoscale Adv.* **2019**, *1*, 3139–3150.
  - (9) Domènech, B.; Kampferbeck, M.; Larsson, E.; Krekeler, T.; Bor, B.; Giuntini, D.; Blankenburg, M.; Ritter, M.; Müller, M.; Vossmeier, T.; Weller, H.; Schneider, G. A. Hierarchical supercrystalline nanocomposites through the self-assembly of organically-modified ceramic nanoparticles. *Sci. Rep.* **2019**, *9*.
  - (10) Feld, A.; Weimer, A.; Kornowski, A.; Winckelmans, N.; Merkl, J.-P.; Kloust, H.; Zierold, R.; Schmidtke, C.; Schotten, T.; Riedner, M.; Bals, S.; Weller, H. Chemistry of Shape-Controlled Iron Oxide Nanocrystal Formation. *ACS Nano* **2018**, *13*, 152–162.
  - (11) Norfolk, L.; Kapusta, K.; Cooke, D.; Staniland, S. Ethylenediamine series as additives to control the morphology of magnetite nanoparticles. *Green Chem.* **2021**, *23*, 5724–5735.

- (12) Plunkett, A.; Temiz, K.; Warren, C.; Wisniewski, V.; Furlan, K. P.; Garay, J.; Giuntini, D.; Domènech, B.; Schneider, G. A. Bridging Nanocrystals to Robust, Multifunctional, Bulk Materials through Nature-Inspired, Hierarchical Design. *pre-print* **2022**,
- (13) Plunkett, A.; Kampfbeck, M.; Bor, B.; Sazama, U.; Krekeler, T.; Bekaert, L.; Noei, H.; Giuntini, D.; Fröba, M.; Stierle, A.; Weller, H.; Vossmeier, T.; Schneider, G. A.; Domènech, B. Strengthening Engineered Nanocrystal Three-Dimensional Superlattices via Ligand Conformation and Reactivity. *ACS Nano* **2022**, *16*, 11692–11707.
- (14) Parkinson, G. S. Iron oxide surfaces. *Surf. Sci. Rep.* **2016**, *71*, 272–365.
- (15) Noh, J.; Osman, O. I.; Aziz, S. G.; Winget, P.; Brédas, J.-L. Magnetite Fe<sub>3</sub>O<sub>4</sub>(111) Surfaces: Impact of Defects on Structure, Stability, and Electronic Properties. *Chem. Mater.* **2015**, *27*, 5856–5867.
- (16) Creutzburg, M.; Sellschopp, K.; Gleißner, R.; Arndt, B.; Vonbun-Feldbauer, G. B.; Vonk, V.; Noei, H.; Stierle, A. Surface structure of magnetite (111) under oxidizing and reducing conditions. *Journal of Physics: Condensed Matter* **2022**, *34*, 164003.
- (17) Kraushofer, F.; Meier, M.; Jakub, Z.; Hütner, J.; Balajka, J.; Hulva, J.; Schmid, M.; Franchini, C.; Diebold, U.; Parkinson, G. S. Oxygen-Terminated (1 × 1) Reconstruction of Reduced Magnetite Fe<sub>3</sub>O<sub>4</sub>(111). *J. Phys. Chem. Lett.* **2023**, *14*, 3258–3265.
- (18) Creutzburg, M.; Sellschopp, K.; Tober, S.; Grånäs, E.; Vonk, V.; Mayr-Schmölzer, W.; Müller, S.; Noei, H.; Vonbun-Feldbauer, G. B.; Stierle, A. Heterogeneous adsorption and local ordering of formate on a magnetite surface. *The Journal of Physical Chemistry Letters* **2021**, *12*, 3847–3852.
- (19) Li, X.; Paier, J. Adsorption of water on the Fe<sub>3</sub>O<sub>4</sub> (111) surface: Structures, stabilities, and vibrational properties studied by density functional theory. *J. Phys. Chem. C* **2016**, *120*, 1056–1065.
- (20) Pentcheva, R.; Wendler, F.; Meyerheim, H. L.; Moritz, W.; Jedrecy, N.; Scheffler, M. Jahn-Teller Stabilization of a “Polar” Metal Oxide Surface: Fe<sub>3</sub>O<sub>4</sub>(001). *Phys. Rev. Lett.* **2005**, *94*, 126101.
- (21) Bliem, R.; McDermott, E.; Ferstl, P.; Setvin, M.; Gamba, O.; Pavelec, J.; Schneider, M.; Schmid, M.; Diebold, U.; Blaha, P., et al. Subsurface cation vacancy stabilization of the magnetite (001) surface. *Science* **2014**, *346*, 1215–1218.

- (22) Parkinson, G. S.; Mulakaluri, N.; Losovyj, Y.; Jacobson, P.; Pentcheva, R.; Diebold, U. Semiconductor–half metal transition at the  $\text{Fe}_3\text{O}_4(001)$  surface upon hydrogen adsorption. *Phys. Rev. B* **2010**, *82*, 125413.
- (23) Gamba, O.; Noei, H.; Pavelec, J.; Bliem, R.; Schmid, M.; Diebold, U.; Stierle, A.; Parkinson, G. S. Adsorption of formic acid on the  $\text{Fe}_3\text{O}_4(001)$  surface. *The Journal of Physical Chemistry C* **2015**, *119*, 20459–20465.
- (24) Arndt, B.; Sellschopp, K.; Creutzburg, M.; Grånäs, E.; Krausert, K.; Vonk, V.; Müller, S.; Noei, H.; Feldbauer, G. B.; Stierle, A. Carboxylic acid induced near-surface restructuring of a magnetite surface. *Communications chemistry* **2019**, *2*, 1–8.
- (25) Liu, H.; Valentin, C. D. Bulk-terminated or reconstructed  $\text{Fe}_3\text{O}_4(001)$  surface: water makes a difference. *Nanoscale* **2018**, *10*, 11021–11027.
- (26) Konuk, M.; Sellschopp, K.; Vonbun-Feldbauer, G. B.; Meißner, R. H. Modeling charge redistribution at magnetite interfaces in empirical force fields. *The journal of physical chemistry C* **2021**, *125*, 4794–4805.
- (27) Creutzburg, M.; Konuk, M.; Tober, S.; Chung, S.; Arndt, B.; Noei, H.; Meißner, R. H.; Stierle, A. Adsorption of oleic acid on magnetite facets. *Communications Chemistry* **2022**, *5*, 1–9.
- (28) Mahmood, A. U.; Yingling, Y. G. All-Atom Simulation Method for Zeeman Alignment and Dipolar Assembly of Magnetic Nanoparticles. *Journal of Chemical Theory and Computation* **2022**, *18*, 3122–3135.
- (29) Mahmood, A. U.; Rizvi, M. H.; Tracy, J. B.; Yingling, Y. G. Solvent Effects in Ligand Stripping Behavior of Colloidal Nanoparticles. *ACS Nano* **2023**, *17*, 13319–13332.
- (30) Butenuth, A.; Moras, G.; Schneider, J.; Koleini, M.; Köppen, S.; Meißner, R.; Wright, L. B.; Walsh, T. R.; Ciacchi, L. C. *Ab initio* derived force-field parameters for molecular dynamics simulations of deprotonated amorphous- $\text{SiO}_2$ /water interfaces. *physica status solidi (b)* **2011**, *249*, 292–305.
- (31) Meißner, R. H.; Konrad, J.; Boll, B.; Fiedler, B.; Zahn, D. Molecular Simulation of Thermosetting Polymer Hardening: Reactive Events Enabled by Controlled Topology Transfer. *Macromolecules* **2020**, *53*, 9698–9705.
- (32) Díaz, D.; Nickel, O.; Moraga, N.; Catalán, R. E.; Retamal, M. J.; Zelada, H.; Cisternas, M.; Meißner, R.; Huber, P.; Corrales, T. P.; Volkmann, U. G. How water wets and

- self-hydrophilizes nanopatterns of physisorbed hydrocarbons. *Journal of Colloid and Interface Science* **2022**, *606*, 57–66.
- (33) Liu, H.; Valentin, C. D. Shaping Magnetite Nanoparticles from First Principles. *Phys. Rev. Lett.* **2019**, *123*.
- (34) Wang, J.; Wolf, R. M.; Caldwell, J. W.; Kollman, P. A.; Case, D. A. Development and testing of a general amber force field. *Journal of Computational Chemistry* **2004**, *25*, 1157–1174.
- (35) Wang, J.; Wolf, R. M.; Caldwell, J. W.; Kollman, P. A.; Case, D. A. Erratum: Junmei Wang, Romain M. Wolf, James W. Caldwell, Peter A. Kollman, and David A. Case, “Development and testing of a general amber force field” *Journal of Computational Chemistry*(2004) 25(9) 1157–1174. *Journal of Computational Chemistry* **2004**, *25*, 1157–1174.
- (36) Cygan, R. T.; Greathouse, J. A.; Kalinichev, A. G. Advances in Clayff Molecular Simulation of Layered and Nanoporous Materials and Their Aqueous Interfaces. *The Journal of Physical Chemistry C* **2021**, *125*, 17573–17589.
- (37) Gürsoy, E.; Vonbun-Feldbauer, G. B.; Meißner, R. H. Oxidation-State Dynamics and Emerging Patterns in Magnetite. *The Journal of Physical Chemistry Letters* **2023**, *14*, 6800–6807.
- (38) Elnaggar, H.; Graas, S.; Lafuerza, S.; Detlefs, B.; Tabiś, W.; Gala, M. A.; Ismail, A.; van der Eerden, A.; Sikora, M.; Honig, J. M.; Glatzel, P.; de Groot, F. Temperature-Driven Self-Doping in Magnetite. *Phys. Rev. Lett.* **2021**, *127*.
- (39) Chambers, S.; Joyce, S. Surface termination, composition and reconstruction of Fe<sub>3</sub>O<sub>4</sub>(001) and  $\gamma$ -Fe<sub>2</sub>O<sub>3</sub>(001). *Surface Science* **1999**, *420*, 111–122.
- (40) Lapkin, D. et al. Defect migration in supercrystalline nanocomposites. To be published.